

Received February 15, 2020, accepted March 16, 2020, date of publication March 25, 2020, date of current version April 13, 2020.

Digital Object Identifier 10.1109/ACCESS.2020.2983181

Low Speed Sensorless Control Based on an Improved Sliding Mode Observation and the Inverter Nonlinearity Compensation for SPMSM

QINGQING YUAN¹, YUMEI YANG¹, HAODONG WU¹, AND HUI WU²

¹Department of Electrical Engineering, University of Shanghai for Science and Technology, Shanghai 200093, China

²China Coal Technology and Engineering Group (CCTEG), Tiandi Science and Technology Company, Ltd., Beijing 100013, China

Corresponding author: Qingqing Yuan (yuanqq@usst.edu.cn)

This work was supported in part by the China Coal Technology and Engineering Group Tiandi Science and Technology Company, Ltd., Youth fund Project under Grant 2018-TD-QN022 and in part by the Shanghai Sailing Program under Grant 18YF1418300.


ABSTRACT It is a difficult to accurately estimate the rotor position in a surface permanent magnet synchronous motor (SPMSM), especially for low speed conditions because the back electromotive force (EMF) is almost zero. In this paper, an improved sliding mode observer (SMO) with a continuous sliding mode switching function (which could reduce the chattering effect) is proposed to estimate the real-time rotor position at a low speed. Through the introduction of an intermediate variable H , the back EMF is extended at low speed, which could improve the estimation accuracy for the rotor position. In addition, the chattering phenomenon is reduced by redesigning the sliding switching function. On the other hand, inverter nonlinearity also results in torque ripple and deteriorates the drive performance because of the harmonic components in the three-phase stator current. Here, a generalized sliding discrete Fourier transform (GSDFT) strategy is studied to extract the harmonic components, which can then be compensated with the corresponding compensation voltage calculated from the motor mathematical model. With the proposed strategy, the estimation accuracy can be apparently restricted when the rotor speed is lower than 50 rpm, while the chattering effect is also improved. With the nonlinearity compensation, the total harmonic distortion obviously decreases, which can improve the rotor estimation and the torque performance. In addition, the GSDFT algorithm executes in approximately half the time of the SDFT compensation method.

INDEX TERMS Surface permanent magnet synchronous motor (SPMSM), low speed, sliding mode observer (SMO), inverter nonlinearity compensation, generalized sliding discrete fourier transform (GSDFT).

I. INTRODUCTION

Currently, permanent magnet synchronous motors (PMSMs) are widely used in various industrial areas for their many advantages. For PMSMs, the high-performance control requires accurate speed and rotor information, which can usually be obtained by mechanical sensors, e.g., rotary or photoelectric encoders [1]. However, with the considerations of cost, installation and harsh environments, these mechanical sensors are not suitable for all occasions, and it is necessary to design sensorless control [2], [3].

Typically, three major kinds of sensorless methods have been widely used for rotor position estimation: (1) methods based on high frequency signal injection, by which the position information is contained in the induced signals

The associate editor coordinating the review of this manuscript and approving it for publication was Fانبiao Li .

because of the motor salient pole effect [4], but this method is unsuitable for surface PMSMs; (2) methods based on motor back EMF, e.g., the model reference adaptive method, sliding mode observer (SMO) method and the Kalman filter method; for example, a new sensorless control strategy based on the combination of the SMO and the extended Kalman filter (EKF) was proposed in [5] to estimate the rotor position, and the chattering effect was improved; and (3) methods based on intelligent algorithms: for example, in [6], the iterative search strategy based on the dichotomy was designed to calculate the back EMF, and the rotor position accuracy was improved because of the successive iterations. In [7], the artificial neural network (ANN) inverse method was used to realize speed observation of a bearingless induction motor.

At present, the research question for sensorless control is how to accurately estimate the rotor position when the speed is low or even zero as the back EMF is almost zero

and the signal-to-noise ratio is low [8], [9]. Considering the robustness and the nonlinear adaptability of the sliding mode control [10], the SMO method is theoretically suitable for sensorless control at a low speed, however, the inherent chattering would affect the control performance. In [11], a second-order SMO with an online resistance estimation was designed to reduce the chattering influence, but the algorithm was complicated.

From another aspect, inverter nonlinearity could also influence the motor performance, as nonlinearity results in harmonic components in the stator currents that certainly deteriorate the torque ripple and the back EMF [12], [13] and affect the estimation of the rotor position. Therefore, essential compensation measurements must be carried out to improve the sensorless control performance. Proper harmonic compensation often requires accurate real-time harmonic extraction or harmonic filtering, which can be generally categorized into two kinds: time-domain methods and frequency-domain methods [14], [15]. Usually, harmonic extraction can be carried out in the frequency domain, in which the discrete Fourier transform and its extension strategies are preferred [16], [17]. Considering that the calculation for the common discrete Fourier transform (DFT) is relatively complicated, a sliding discrete Fourier transform (SDFT) was proposed in [18], [19], which improved the speed of harmonic extraction and was suitable for digital implementation. Although the SDFT is computationally efficient, this method still might have drawbacks, e.g., slow dynamic performance and sensitivity to the frequency variation, and a generalized discrete Fourier transform (GDFT) was researched in [20]; with the reconstruction of the common DFT, signal extraction has been realized with great performance and flexibility.

In this paper, a novel sensorless control strategy suitable for low speed conditions is researched for SPMSMs based on an improved SMO and inverter nonlinearity compensation. First, an intermediate variable H is introduced to the improved SMO to extend the back EMF at low speed, which could improve the estimation accuracy, and a new sliding switching function is redesigned to reduce the chattering phenomenon. Then, a generalized SDFT (GSDFT) strategy is proposed to realize fast harmonic extraction, based on which the corresponding compensation voltage can be generated and involved in a compensation loop to improve the stator current performance and the estimation accuracy of the rotor position.

The structure of this paper is as follows. This new SMO is designed in Section II. The influence of inverter nonlinearity, the harmonic extraction with GSDFT and the corresponding compensation method are introduced in Section III in detail. Section IV contains the results analysis and comparison, while the conclusion and outlook are given in Section V.

II. SLIDING MODE OBSERVATION

Sliding mode control is a typical nonlinear control system, whose performance usually lies in the selection of the sliding

mode control laws, and this system is necessary to avoid the excessive chattering.

A. CONVENTIONAL METHOD

Basically, the design of the traditional SMO is based on a mathematical model. For the SPMSM, the voltage equations in the $\alpha\beta$ coordinates are as follows [21]

$$\begin{bmatrix} u_\alpha \\ u_\beta \end{bmatrix} = \begin{bmatrix} R + pL_s & 0 \\ 0 & R + pL_s \end{bmatrix} \begin{bmatrix} i_\alpha \\ i_\beta \end{bmatrix} + \begin{bmatrix} E_\alpha \\ E_\beta \end{bmatrix} \quad (1)$$

where L_s is the stator inductance; u_α, u_β and i_α, i_β are the stator voltages and currents in the $\alpha\beta$ coordinates, respectively; E_α, E_β are the EMF components and p is the differential operator. The EMF components can be represented as

$$\begin{bmatrix} E_\alpha \\ E_\beta \end{bmatrix} = \omega_e \Psi_f \begin{bmatrix} -\sin \theta_e \\ \cos \theta_e \end{bmatrix} \quad (2)$$

where ω_e is the electrical angular velocity, Ψ_f is the amplitude of the magnetic flux linkage in each phase and θ_e is the electrical rotor position.

From equation (2), it is obvious that the rotor position θ_e can be estimated if the back EMF has been obtained at high accuracy. Here, SMO is used to observe the back EMF value, and the voltage equation is rewritten as

$$\frac{d}{dt} \begin{bmatrix} i_\alpha \\ i_\beta \end{bmatrix} = \frac{1}{L_s} \begin{bmatrix} -R & 0 \\ 0 & -R \end{bmatrix} \begin{bmatrix} i_\alpha \\ i_\beta \end{bmatrix} + \frac{1}{L_s} \begin{bmatrix} u_\alpha \\ u_\beta \end{bmatrix} - \frac{1}{L_s} \begin{bmatrix} E_\alpha \\ E_\beta \end{bmatrix} \quad (3)$$

Assuming that $\hat{i}_\alpha, \hat{i}_\beta$ are the observed stator current components from SMO, u_α, u_β are taken as the control input of the observer, and v_α, v_β are the sliding mode control laws to be chosen, then the traditional SMO can be represented as

$$\frac{d}{dt} \begin{bmatrix} \hat{i}_\alpha \\ \hat{i}_\beta \end{bmatrix} = \frac{1}{L_s} \begin{bmatrix} -R & 0 \\ 0 & -R \end{bmatrix} \begin{bmatrix} \hat{i}_\alpha \\ \hat{i}_\beta \end{bmatrix} + \frac{1}{L_s} \begin{bmatrix} u_\alpha \\ u_\beta \end{bmatrix} - \frac{1}{L_s} \begin{bmatrix} v_\alpha \\ v_\beta \end{bmatrix} \quad (4)$$

Taking the difference between equations (3) and (4), the error equation can be settled as

$$\frac{d}{dt} \begin{bmatrix} \tilde{i}_\alpha \\ \tilde{i}_\beta \end{bmatrix} = \frac{1}{L_s} \begin{bmatrix} -R & 0 \\ 0 & -R \end{bmatrix} \begin{bmatrix} \tilde{i}_\alpha \\ \tilde{i}_\beta \end{bmatrix} + \frac{1}{L_s} \begin{bmatrix} E_\alpha - v_\alpha \\ E_\beta - v_\beta \end{bmatrix} \quad (5)$$

where $\tilde{i}_\alpha = \hat{i}_\alpha - i_\alpha, \tilde{i}_\beta = \hat{i}_\beta - i_\beta$ are the current observation errors in $\alpha\beta$ coordinates respectively and the traditional sliding mode control laws are usually set as following

$$\begin{bmatrix} v_\alpha \\ v_\beta \end{bmatrix} = \begin{bmatrix} k \operatorname{sgn}(\hat{i}_\alpha - i_\alpha) \\ k \operatorname{sgn}(\hat{i}_\beta - i_\beta) \end{bmatrix} \quad (6)$$

where k is the sliding mode gain designed according to the Lyapunov stability principle.

When the state variables of the observer (here preferring \tilde{i}_α and \tilde{i}_β) reach the sliding surface, that means $\tilde{i}_\alpha = 0$ and $\tilde{i}_\beta = 0$, and the observer state remains on the sliding surface; in addition, the derivations of the current error are also zero,

which means that equation (5) = 0, then the back EMF can be obtained by equations (5) and (6) as follows

$$\begin{bmatrix} \hat{E}_\alpha \\ \hat{E}_\beta \end{bmatrix} = \begin{bmatrix} v_\alpha \\ v_\beta \end{bmatrix} = \begin{bmatrix} k \operatorname{sgn}(\tilde{i}_\alpha) \\ k \operatorname{sgn}(\tilde{i}_\beta) \end{bmatrix} \quad (7)$$

With equation (2), the rotor position can be obtained as

$$\hat{\theta}_{\text{eq}} = -\arctan(\hat{E}_\alpha / \hat{E}_\beta) \quad (8)$$

where “^” represents the observation value.

Since the actual control variable is a discontinuous high frequency switching signal, a low-pass filter is usually needed to extract the continuous back EMF. Considering that the phase delay that results from the low-pass filter, an angle compensation is added as follows

$$\hat{\theta}_e = \hat{\theta}_{\text{eq}} + \arctan(\hat{\omega}_e / \omega_c) \quad (9)$$

where ω_c is the cutoff frequency of the low pass filter, and the estimated electrical angular velocity can be obtained from equation (2).

$$\hat{\omega}_e = \frac{\sqrt{\hat{E}_\alpha^2 + \hat{E}_\beta^2}}{\psi_f} \quad (10)$$

The control diagram of the traditional SMO is shown in Figure 1.

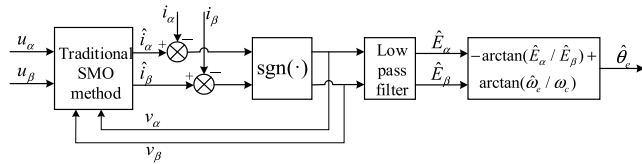


FIGURE 1. Block diagram of a traditional SMO.

B. IMPROVED METHOD

For the conventional method, when the motor runs at a low speed, the back EMF is almost zero and the estimation accuracy is certainly reduced because of the low signal-to-noise ratio. Here, a way to extend the back EMF is proposed that introduces an intermediate variable “H”.

Similarly, assuming that \hat{i}_α and \hat{i}_β are the observed stator current components from the new SMO, the newly SMO could be represented as

$$\begin{aligned} \frac{d}{dt} \begin{bmatrix} \hat{i}_\alpha \\ \hat{i}_\beta \end{bmatrix} &= A \begin{bmatrix} \hat{i}_\alpha \\ \hat{i}_\beta \end{bmatrix} + \frac{1}{L_s} \begin{bmatrix} u_\alpha \\ u_\beta \end{bmatrix} \\ &\quad - \frac{1}{L_s} \begin{bmatrix} K \operatorname{sigmoid}(\hat{i}_\alpha - i_\alpha) \\ K \operatorname{sigmoid}(\hat{i}_\beta - i_\beta) \end{bmatrix} + \frac{1}{2L_s} H \end{aligned} \quad (11)$$

where

$$A = \begin{bmatrix} -\frac{R}{L_s} & 0 \\ 0 & -\frac{R}{L_s} \end{bmatrix}, \quad H = \frac{\omega_c}{s + \omega_c} \begin{bmatrix} K \operatorname{sigmoid}(\hat{i}_\alpha - i_\alpha) \\ K \operatorname{sigmoid}(\hat{i}_\beta - i_\beta) \end{bmatrix}$$

$\operatorname{sigmoid}(x) = \frac{2}{1+e^{-ax}} - 1$, K is the sliding mode gain. Here, H is designed to extend the back EMF.

Taking difference between equations (3) and (11), the error equation can be represented by

$$\begin{aligned} \frac{d}{dt} \begin{bmatrix} \tilde{i}_\alpha \\ \tilde{i}_\beta \end{bmatrix} &= A \begin{bmatrix} \tilde{i}_\alpha \\ \tilde{i}_\beta \end{bmatrix} - \frac{1}{L_s} \begin{bmatrix} K \operatorname{sigmoid}(\tilde{i}_\alpha) \\ K \operatorname{sigmoid}(\tilde{i}_\beta) \end{bmatrix} \\ &\quad + \frac{1}{2L_s} H + \frac{1}{L_s} \begin{bmatrix} E_\alpha \\ E_\beta \end{bmatrix} \end{aligned} \quad (12)$$

In the same way, when the state variables of the observer reach the sliding surface, the observer state remains on the sliding surface; in addition, the derivations of the current error are also zero, which means that equation (12) = 0, then the back EMF can be obtained by equations (12) as follows

$$\begin{aligned} \begin{bmatrix} \hat{E}_\alpha \\ \hat{E}_\beta \end{bmatrix} &= \begin{bmatrix} K \operatorname{sigmoid}(\tilde{i}_\alpha) \\ K \operatorname{sigmoid}(\tilde{i}_\beta) \end{bmatrix} - \frac{1}{2} H \\ &= \left(1 - \frac{\omega_c}{2s + 2\omega_c}\right) \begin{bmatrix} K \operatorname{sigmoid}(\tilde{i}_\alpha) \\ K \operatorname{sigmoid}(\tilde{i}_\beta) \end{bmatrix} \end{aligned} \quad (13)$$

Considering that ω_c is much larger than the speed ω_e , equation (13) can be simplified as

$$\begin{bmatrix} \hat{E}_\alpha \\ \hat{E}_\beta \end{bmatrix} = \frac{1}{2} \begin{bmatrix} K \operatorname{sigmoid}(\tilde{i}_\alpha) \\ K \operatorname{sigmoid}(\tilde{i}_\beta) \end{bmatrix} = \frac{1}{2} \begin{bmatrix} H_\alpha \\ H_\beta \end{bmatrix} \quad (14)$$

Obviously, the value of H is the twice that of the back EMF, hence, H is used to replace the back EMF to estimate the rotor position, which apparently doubles the back EMF and is suitable for low-speed rotor position estimation.

With the consideration of the phase delay compensation, the estimated rotor position can then be formulated as

$$\hat{\theta}_e = \arctan\left(-\frac{H_\alpha}{H_\beta}\right) + \arctan\left(\frac{\hat{\omega}_e}{\omega_c}\right) \quad (15)$$

To analyze the stability of the new SMO, the Lyapunov function [22] is chosen as

$$V = \frac{1}{2} s_\alpha^2 + \frac{1}{2} s_\beta^2 \quad (16)$$

where $s_\alpha = \hat{i}_\alpha - i_\alpha$, $s_\beta = \hat{i}_\beta - i_\beta$ is the designed sliding surface.

Taking the derivative of equation (16) and substituting equation (12) into the derivation, then

$$\begin{aligned} \dot{V} &= s_\alpha \dot{s}_\alpha + s_\beta \dot{s}_\beta = -\frac{R}{L_s} (s_\alpha^2 + s_\beta^2) \\ &\quad + \frac{1}{L_s} [s_\alpha (E_\alpha - K \operatorname{sigmoid}(s_\alpha) + \frac{K \omega_c \operatorname{sigmoid}(s_\alpha)}{2s + 2\omega_c}) \\ &\quad + s_\beta (E_\beta - K \operatorname{sigmoid}(s_\beta) + \frac{K \omega_c \operatorname{sigmoid}(s_\beta)}{2s + 2\omega_c})] \end{aligned} \quad (17)$$

According to Lyapunov’s theorem, the new SMO is stable when $\dot{V} < 0$; therefore, the stability conditions can be deduced as follows

$$K > \max\{|2E_\alpha|, |2E_\beta|\} \quad (18)$$

It can be seen that as long as the sliding mode gain K is large enough, the stability of the novel SMO can be guaranteed.

III. NONLINEAR HARMONIC COMPENSATION

A. HARMONIC INFLUENCE

Because of the inverter nonlinearity, e.g., dead-zone time, saturation on-voltage drop of switching devices, and pulse width modulation, there are harmonic components in the stator currents, which also affects the estimation accuracy of the rotor position [23]–[25].

For example, for a rotor speed $n = 10\text{rpm}$, the three-phase stator currents are shown in Figure 2(a), and the harmonic distortion of the A-phase is shown in Figure 2(b). Obviously, there are $(6k \pm 1)^{\text{th}}$ harmonic components and the low-order harmonics are relatively large (5th: 4.08%; 7th: 4.11%, and the total harmonic distortion (THD) is 8.06%), which affects the back-EMF estimation because the signal-to-noise ratio decreases.

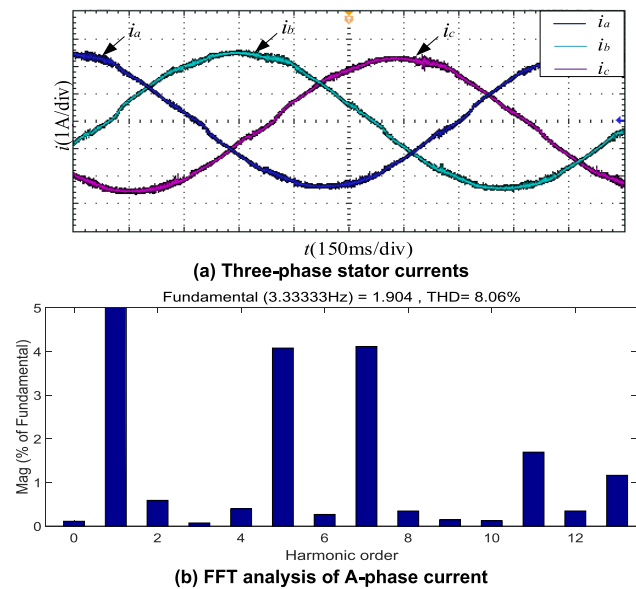


FIGURE 2. Inverter nonlinearity influence on the stator currents.

To improve the estimation performance of the rotor position, these current harmonic components should be accurately extracted and compensated. In this paper, a new harmonic extraction algorithm named the generalized sliding discrete Fourier transform (GSDFT) is studied.

B. HARMONIC EXTRACTION METHOD—GSDFT

Basically, GSDFT has the same characteristics as the normal sliding discrete Fourier transform (SDFT) with better dynamic performance and robustness.

Assuming that the stator current is a finite data sequence that is expressed as $i(m)$ and its length is M , its discrete Fourier transform can be written as

$$I(k) = \text{DFT}[i(m)] = \sum_{n=0}^{M-1} i(m)W_M^{nk}, \quad (0 \leq k \leq M-1) \quad (19)$$

where $W_M = e^{-j2\pi/M}$.

Equation (19) can be mathematically expressed as

$$I(k) = i(0) + i(1)e^{-j\frac{2\pi k}{M}} + i(2)e^{-j\frac{2\pi k \cdot 2}{M}} + \dots + i(M-1)e^{-j\frac{2\pi k \cdot (M-1)}{M}} \quad (20)$$

Suppose that the first sampling data M are $i(0) \sim i(M-1)$, and the first sequence is represented by i_0 whose DFT is represented by $I_0(k)$, and suppose that the second sampling data M are $i(1) \sim i(M)$, the corresponding sequence is i_1 , and the DFT is $I_1(k)$. The data processing is shown in Figure 3.

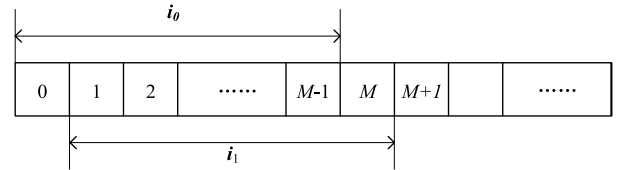


FIGURE 3. Schematic diagram of discrete data processing.

Apparently,

$$\begin{aligned} I_1(k) &= [I_0(k) - i(0)]e^{j\frac{2\pi k}{M}} + i(M)e^{-j\frac{2\pi k(M-1)}{M}} \\ &= [I_0(k) - i(0) + i(M)]e^{j\frac{2\pi k}{M}} \end{aligned} \quad (21)$$

Equation (21) is the SDFT algorithm which is suitable for the digital implementation, and the specific harmonic amplitude can be read by setting a specific k value.

The SDFT of the m^{th} sequence is

$$I_m(k) = [I_{m-1}(k) - i(m-1) + i(m+M-1)]e^{j\frac{2\pi k}{M}} \quad (22)$$

where $I_m(k)$ is the k^{th} harmonic component of the m^{th} sequence, in detail, referring to $i(m) \sim i(m+M-1)$ and $I_{m-1}(k)$ is the k^{th} harmonic component of the previous $(m-1)^{\text{th}}$ sequence $i(m-1) \sim i(m+M-2)$.

In the time-domain, the k^{th} harmonic of the m^{th} sequence can be written as

$$i^k(m) = \frac{1}{M} I_m(k) e^{j2\pi \frac{km}{M}} \quad (23)$$

Supposing that the m^{th} sequence is the input signal and the extracted k^{th} harmonic component is the output signal, the transfer function in z-domain is as follows

$$\begin{aligned} G^k(z) &= \frac{Z[\frac{1}{M} I_m(k) e^{j2\pi \frac{km}{M}}]}{Z[i(k)]} \\ &= (1 - z^{-M}) \left(\frac{1}{1 - z^{-1} e^{j2\pi \frac{k}{M}}} \right) \frac{1}{M} e^{j2\pi \frac{k}{M}} \end{aligned} \quad (24)$$

Set

$$H_c(z) = 1 - z^{-M} = \prod_{n=0}^{M-1} (1 - e^{j2\pi \frac{n}{M}} z^{-1}) \quad (25)$$

There are three parts in the transfer function (equation (24)), as shown in Figure 4: $H_c(z)$, for which equation (25) shows that this part introduces M zero points centered on $\omega = \lambda\omega_0$, where $\omega_0 = 2\pi/M$, $\lambda = 0, 1, \dots, M-1$, and evenly distributed on the unit circle to achieve complete elimination of the corresponding frequency harmonics. The second part produces a pole. When $\omega = k\omega_0$, the poles and zeros cancel each other, achieving zero attenuation and zero phase shift of the k^{th} harmonic and then extracting the k^{th} harmonic. The third part adjusts the amplitude of the k^{th} harmonic [20].

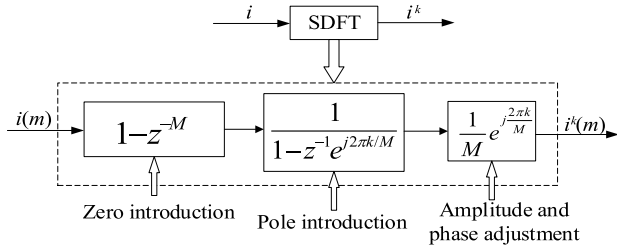


FIGURE 4. Structure diagram of the SDFT algorithm.

The corresponding pole-zero diagram for $M = 24$ and $k = 5$ is shown in Figure 5.

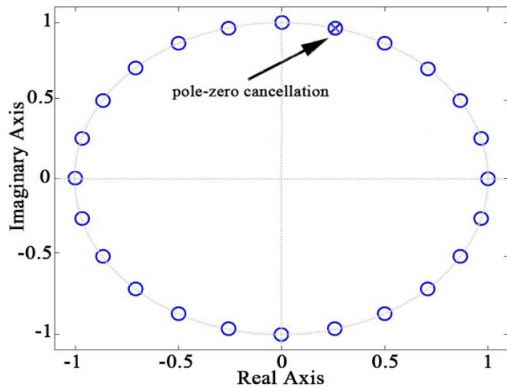


FIGURE 5. Pole-zero diagram of the SDFT algorithm ($M=24$ and $k=5$).

Apparently, the $H_c(z)$ part is very important, mainly in two ways: 1) $H_c(z)$ determines which harmonic components are completely filtered out. In equation (25), $H_c(z)$ introduces zeros at all the integer multiples of the fundamental frequency, e.g., $\omega = \lambda\omega_0$ ($\lambda = 0, 1, \dots, M-1$); therefore, all the integer harmonics can be completely filtered out, which might cause zero redundancy for the harmonic conditions studied in this paper. 2) $H_c(z)$ determines the dynamic response performance of the harmonic extraction. Introducing M zero points means M delay links and results in unnecessary time delay, which is a drawback of the SDFT algorithm.

To improve the response performance, the generalized sliding discrete Fourier transform (GSDFT) is studied here by redesigning $H_c(z)$. Considering that, the harmonic orders to be eliminated in this paper can be represented as $k = 6h \pm 1$ ($h = 1, 2, 3, \dots$), $H_c(z)$ in equation (25) can be redesigned as $z = z^{1/6} e^{-j2\pi/6M}$; in detail, $H_c(z)$ is redesigned as

$$H_c(z) = (1 - z^{-\frac{M}{6}} e^{j\frac{2\pi}{6}})(1 - z^{-\frac{M}{6}} e^{-j\frac{2\pi}{6}}) \prod_{n=0}^{N-1} (1 - e^{j2\pi \frac{6k+1}{6M}} z^{-\frac{1}{6}}) \prod_{n=0}^{N-1} (1 - e^{j2\pi \frac{6k-1}{6M}} z^{-\frac{1}{6}}) \quad (26)$$

The transfer function of GSDFT can be rewritten as

$$G_S^k(z) = (1 - z^{-\frac{M}{6}} e^{j\frac{2\pi}{6}})(1 - z^{-\frac{M}{6}} e^{-j\frac{2\pi}{6}}) \times \left(\frac{1}{1 - z^{-1} e^{j2\pi \frac{k}{M}}} \right) \frac{1}{M} e^{j2\pi \frac{k}{M}} \quad (27)$$

The zero center of the GSDFT algorithm becomes $\omega = (6h \pm 1)\omega_0$, and the number of system zero points becomes $M/6 + M/6 = M/3$. Compared with SDFT, the number of zeros is one third that of the original, which means the delay time of GSDFT is also reduced to one third that of SDFT. The corresponding structure diagram of the GSDFT algorithm is shown in Figure 6, and the corresponding pole-zero diagram when $M = 24$ and $k = 5$ is shown in Figure 7.

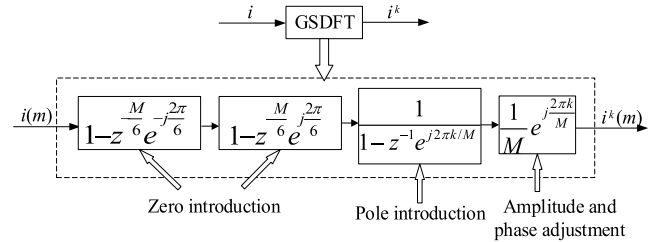


FIGURE 6. Structure diagram of the GSDFT algorithm.

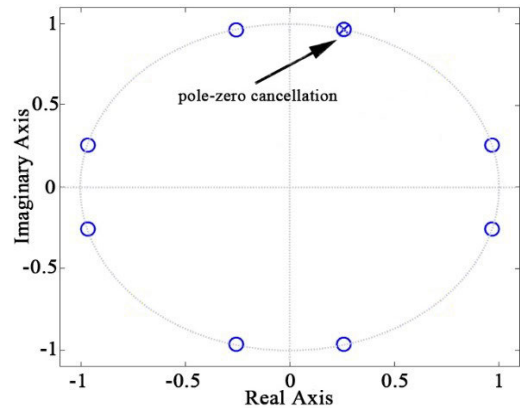


FIGURE 7. Pole-zero diagram of the GSDFT algorithm ($M=24$ and $k=5$).

C. HARMONIC COMPENSATION

After the extraction of the harmonic current components, the corresponding compensation voltage can then be calculated based on the motor mathematical models.

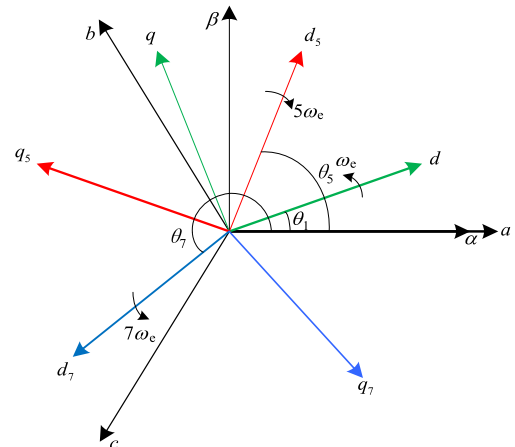


FIGURE 8. Harmonic coordinates system.

First, a harmonic coordinate system is established as shown in Figure 8 (here, only dealing with the 5th and 7th components), and the harmonic current components in rotating coordinates (dq coordinates) are represented as

$$\begin{cases} i_d = i_{d1} + I_5 \cos(-6\omega_e t + \theta_5) + I_7 \cos(6\omega_e t + \theta_7) \\ i_q = i_{q1} + I_5 \sin(-6\omega_e t + \theta_5) + I_7 \sin(6\omega_e t + \theta_7) \end{cases} \quad (28)$$

where i_d and i_q are the stator currents in dq coordinates and i_{d1} and i_{q1} are the fundamental current components. I_5 and I_7 are the amplitudes of the fundamental, 5th and 7th harmonic currents, respectively; θ_5 and θ_7 are initial phase angles of the fundamental, 5th and 7th harmonic currents respectively. In addition, the angular frequencies of the 5th and 7th are $-6\omega_e$ and $6\omega_e$ respectively, in dq coordinates.

For the ideal case, the voltage equations of SPMSM in the dq coordinates are as follows

$$\begin{aligned} u_d^* &= R i_{d1} - \omega_e L_q i_{q1} + L_d p i_{d1} \\ u_q^* &= R i_{q1} + \omega_e L_d i_{d1} + L_q p i_{q1} + \omega_e \psi_f \end{aligned} \quad (29)$$

While with the consideration of the harmonic components, the actual voltage equations can be written as

$$\begin{cases} u_d = R [i_{d1} + I_5 \cos(-6\omega_e t + \theta_5) + I_7 \cos(6\omega_e t + \theta_7)] \\ \quad - \omega_e L_q [i_{q1} + I_5 \sin(-6\omega_e t + \theta_5) + I_7 \sin(6\omega_e t + \theta_7)] \\ \quad + L_d [p i_{d1} + 6\omega_e I_5 \sin(-6\omega_e t + \theta_5) - 6\omega_e I_7 \sin(6\omega_e t + \theta_7)] \\ u_q = R [i_{q1} + I_5 \sin(-6\omega_e t + \theta_5) + I_7 \sin(6\omega_e t + \theta_7)] \\ \quad + \omega_e L_d [i_{d1} + I_5 \cos(-6\omega_e t + \theta_5) + I_7 \cos(6\omega_e t + \theta_7)] \\ \quad + L_q [p i_{q1} - 6\omega_e I_5 \cos(-6\omega_e t + \theta_5) + 6\omega_e I_7 \cos(6\omega_e t + \theta_7)] \\ \quad + \omega_e \psi_f \end{cases} \quad (30)$$

In which L_d and L_q are the direct and quadrature inductances, respectively.

Therefore, the voltage deviations to be compensated are

$$\begin{cases} \Delta u_d = u_d^* - u_d \\ = -R [I_5 \cos(-6\omega_e t + \theta_5) + I_7 \cos(6\omega_e t + \theta_7)] \\ \quad + \omega_e L_q [I_5 \sin(-6\omega_e t + \theta_5) + I_7 \sin(6\omega_e t + \theta_7)] \\ \quad - L_d [6\omega_e I_5 \sin(-6\omega_e t + \theta_5) - 6\omega_e I_7 \sin(6\omega_e t + \theta_7)] \\ \Delta u_q = u_q^* - u_q \\ = -R [I_5 \sin(-6\omega_e t + \theta_5) + I_7 \sin(6\omega_e t + \theta_7)] \\ \quad - \omega_e L_d [I_5 \cos(-6\omega_e t + \theta_5) + I_7 \cos(6\omega_e t + \theta_7)] \\ \quad - L_q [-6\omega_e I_5 \cos(-6\omega_e t + \theta_5) + 6\omega_e I_7 \cos(6\omega_e t + \theta_7)] \end{cases} \quad (31)$$

It is hard to obtain these time-dependent quantities equation (31), e.g., $6\omega_e t$, which can be solved based on the harmonic coordinates, as shown in Figure 8, and the transformation matrixes are as follows

$$C_{dq \rightarrow dq5} = \begin{bmatrix} \cos(-6\omega_e t) & \sin(-6\omega_e t) \\ -\sin(-6\omega_e t) & \cos(-6\omega_e t) \end{bmatrix} \quad (32)$$

$$C_{dq \rightarrow dq7} = \begin{bmatrix} \cos(6\omega_e t) & \sin(6\omega_e t) \\ -\sin(6\omega_e t) & \cos(6\omega_e t) \end{bmatrix} \quad (33)$$

Then, the voltage deviations in equation (31) can be transformed as equations (34) and (35), in which $L_s = L_d = L_q$.

$$\begin{cases} \Delta u_{d5} = -R [I_5 \cos \theta_5 + I_7 \cos(12\omega_e t + \theta_7)] \\ \quad + \omega_e L_s [I_5 \sin \theta_5 + I_7 \sin(12\omega_e t + \theta_7)] \\ \quad - L_s [6\omega_e I_5 \sin \theta_5 - 6\omega_e I_7 \sin(12\omega_e t + \theta_7)] \\ \Delta u_{q5} = -R [I_5 \sin \theta_5 + I_7 \sin(12\omega_e t + \theta_7)] \\ \quad - \omega_e L_s [I_5 \cos \theta_5 + I_7 \cos(12\omega_e t + \theta_7)] \\ \quad + L_s [6\omega_e I_5 \cos \theta_5 - 6\omega_e I_7 \cos(12\omega_e t + \theta_7)] \end{cases} \quad (34)$$

$$\begin{cases} \Delta u_{d7} = -R [I_5 \cos(-12\omega_e t + \theta_5) + I_7 \cos \theta_7] \\ \quad + \omega_e L_s [I_5 \sin(-12\omega_e t + \theta_5) + I_7 \sin \theta_7] \\ \quad - L_s [6\omega_e I_5 \sin(-12\omega_e t + \theta_5) - 6\omega_e I_7 \sin \theta_7] \\ \Delta u_{q7} = -R [I_5 \sin(-12\omega_e t + \theta_5) + I_7 \sin \theta_7] \\ \quad - \omega_e L_s [I_5 \cos(-12\omega_e t + \theta_5) + I_7 \cos \theta_7] \\ \quad + L_s [6\omega_e I_5 \cos(-12\omega_e t + \theta_5) - 6\omega_e I_7 \cos \theta_7] \end{cases} \quad (35)$$

Obviously, both DC and AC ($12\omega_e t$) components exist in the compensation voltages. Considering that these AC components are easily eliminated, the final compensation voltages can be expressed as

$$\begin{cases} u_{d5}^{com} = -R I_5 \cos \theta_5 - 5\omega_e L_s I_5 \sin \theta_5 \\ u_{q5}^{com} = -R I_5 \sin \theta_5 + 5\omega_e L_s I_5 \cos \theta_5 \end{cases} \quad (36)$$

$$\begin{cases} u_{d7}^{com} = -R I_7 \cos \theta_7 + 7\omega_e L_s I_7 \sin \theta_7 \\ u_{q7}^{com} = -R I_7 \sin \theta_7 - 7\omega_e L_s I_7 \cos \theta_7 \end{cases} \quad (37)$$

Thus, the whole control structure is shown in Figure 9.

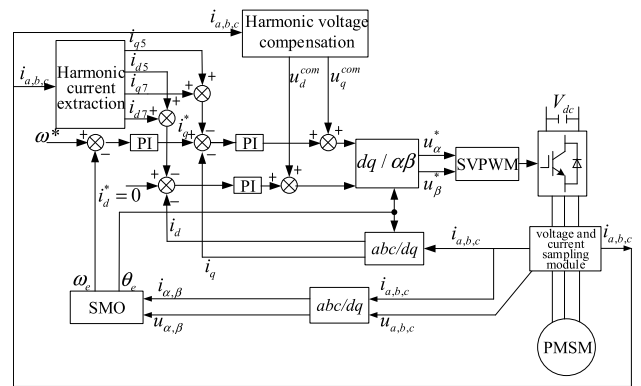


FIGURE 9. Block diagram of the whole control structure.

IV. EXPERIMENTAL RESULTS

To verify the effectiveness of the proposed the low speed sensorless control strategy, an experimental platform was established, as displayed in Figure 10, whose detailed parameters are listed in Table 1.

A. COMPARISONS BETWEEN GSDFT AND SDFT ALGORITHMS

1) DYNAMIC RESPONSE

With a static input signal $i_{in} = \sin 500\pi t$, the tracking waveforms of GSDFT and SDFT are compared in Figure 11.

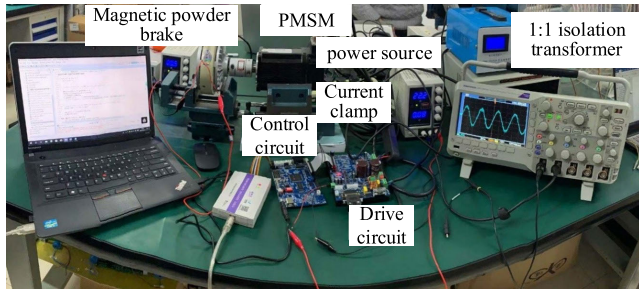


FIGURE 10. Experimental platform.

TABLE 1. Detailed parameters for SPMSM.

Parameter name	Parameter value
Resistance(R)	2.8750 Ω
Rotor flux linkage(ψ_r)	0.175 Wb
Straight axis inductance(L_d)	8.5 mH
Cross-axis inductance(L_q)	8.5 mH
Moment of inertia(J)	0.05 kg/m ²
Motor pole pair(p)	4

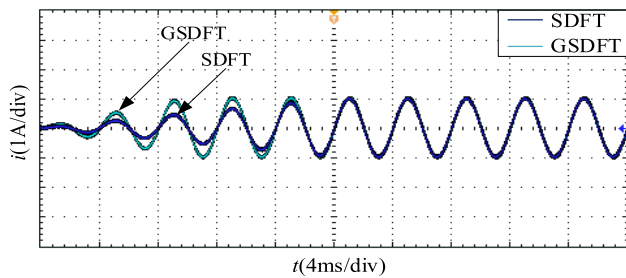


FIGURE 11. Tracking waveforms with a static input.

Obviously, the tracking time of GSDFT is approximately two cycles while being approximately five cycles for SDFT. When $t = 0.2s$, the input amplitude is doubled(1A→2A), and the dynamic tracking results are shown in Figure 12.

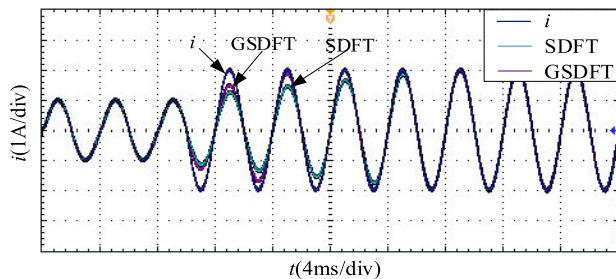


FIGURE 12. Dynamic voltage waveforms.

Similarly, for GSDFT, the dynamic response time is approximately two cycles while being approximately five cycles for SDFT.

For the GSDFT and SDFT algorithms, the execution times of the extraction of 5th and 7th harmonic components are compared in Table 2.

TABLE 2. Comparison of harmonic extraction times.

Harmonic extraction method	5 th harmonic extraction time (μs)	7 th harmonic extraction time (μs)
SDFT	157.28	143.22
GSDFT	87.19	78.62

TABLE 3. Comparisons of the extraction results.

Harmonic extraction method	5 th harmonic (percentage)	7 th harmonic (percentage)
SDFT	4.61%	4.34%
GSDFT	4.60%	4.34%

The GSDFT algorithm has an approximately 44.82% time savings compared with SDFT.

2) HARMONIC EXTRACTION COMPARISONS

With the stator currents in Figure 2 as an example, the harmonic extraction results from different methods are shown in Table 3.

Apparently, the SDFT and GSDFT algorithms are identical regarding harmonic extraction.

The conclusions of the above experimental results can be summarized as

(1) This GSDFT method has the same steady extraction performance as the normal SDFT method, which means the steady stator current performances of the different methods are the same.

(2) The dynamic response of the GSDFT is approximately 2-3 signal cycles faster than that of the SDFT, which is conducive to the digital implementation.

B. STABILITY EXPERIMENTS ON NEW SMO AND CONVENTIONAL SMO

1) SPEED MUTATION

The experiments are carried out according to the following procedures to make verifications and comparisons.

(1) At $t = 0s$, the SPMSM has a full load starting from 0rpm to 10rpm;

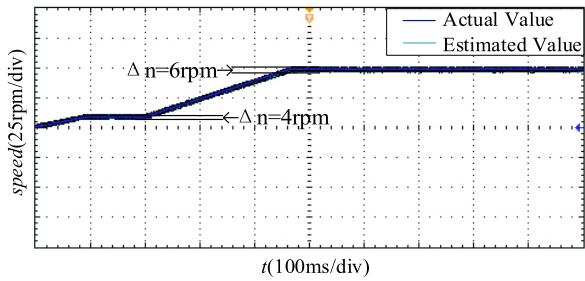
(2) At $t = 0.2s$, the speed abruptly changes from 10rpm to 50rpm.

The estimation results with the conventional and new SMO methods are shown in Figures 13 and 14.

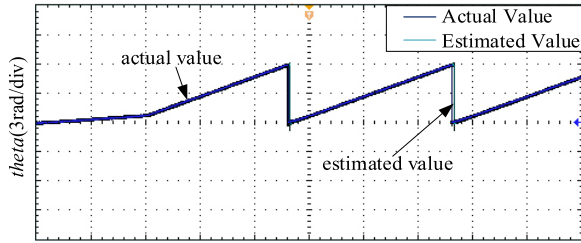
According to Figure 13 and 14, when the rotor speed is 50 rpm, the estimation errors are within ± 6 rpm and ± 3 rpm for the conventional and new SMOs while being ± 4 rpm and ± 1.5 rpm for each when the rotor speed is 10rpm, which proves the effectiveness of this new SMO.

2) LOAD MUTATION

The load mutation experiments are carried out according to the following procedures.

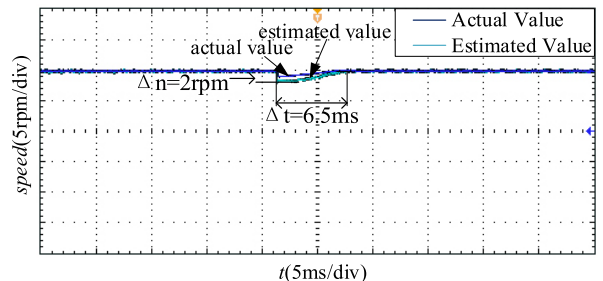


(a) Speed estimation

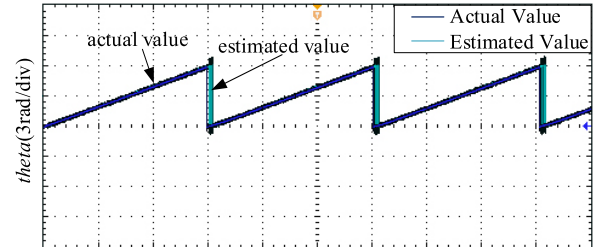


(b) Rotor position estimation

FIGURE 13. Estimation results of the conventional SMO.

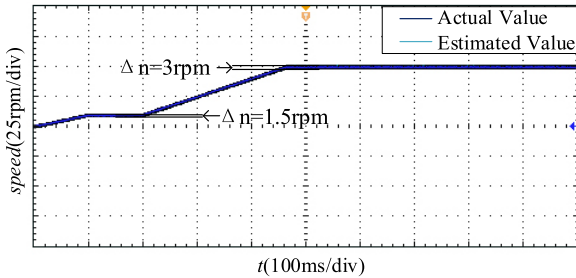


(a) Speed estimation

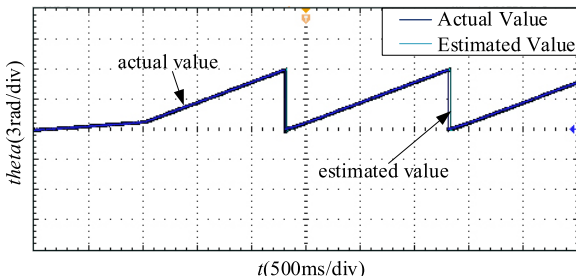


(b) Rotor position estimation

FIGURE 15. Estimation results of the conventional SMO.

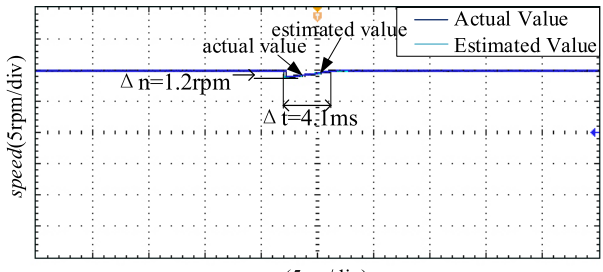


(a) Speed estimation

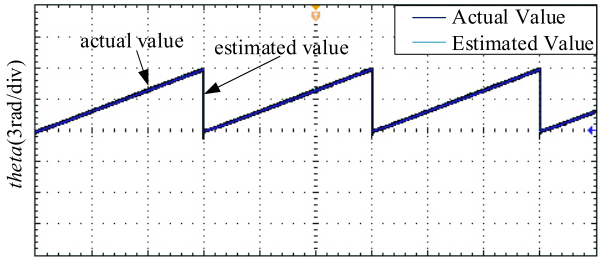


(b) Rotor position estimation

FIGURE 14. Estimation results of the new SMO.



(a) Speed estimation



(b) Rotor position estimation

FIGURE 16. Estimation results of the new SMO.

- (1) First, SPMSM runs stably at the 10 rpm;
- (2) At $t = 0.2s$, the load abruptly changes from 0N.m to the rated value.

The estimation results from the conventional and new SMO methods are shown in Figures 15 and 16.

According to Figures 15 and 16, when the load abruptly changes from 0 N.m to the rated value, the dynamic response times are 6.5 ms and 4.1 ms for the conventional and new SMOs respectively, and for the estimation error, thi new SMO has better performance than the conventional one.

3) CHATTERING COMPARISONS

When sliding surface $\tilde{i}_\alpha = 0$, the estimated stator value is equal to the real value. Here, taking the estimated stator

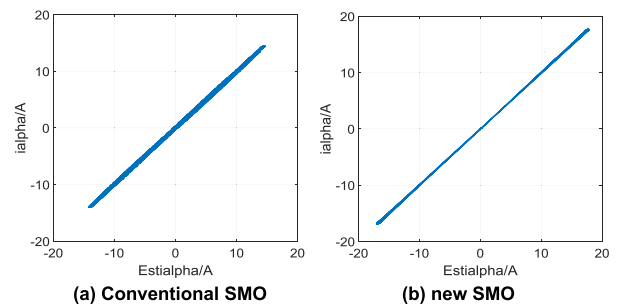


FIGURE 17. Chattering comparison for the different SMO strategies.

current as the x-coordinate and the real value as the y-coordinate, the trajectories of the sliding surface for the

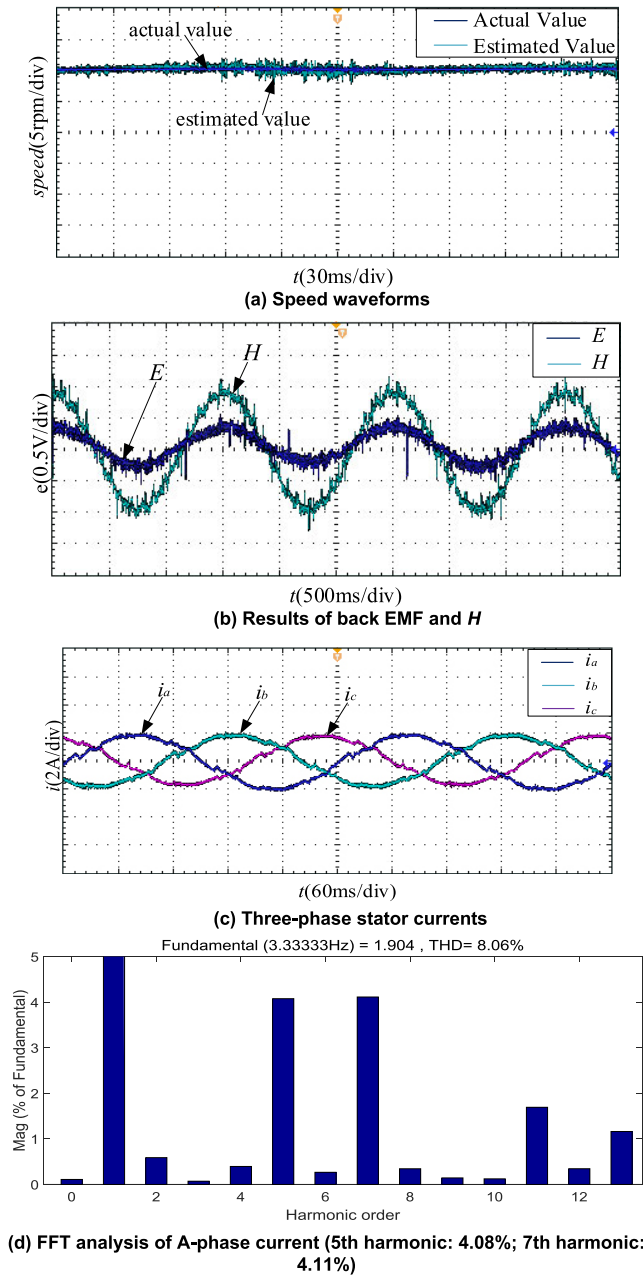


FIGURE 18. Results without nonlinearity compensation.

different SMO strategies can be compared in Figure 17. It can be seen that the chattering is improved considerably by the new SMO.

C. SENSORLESS CONTROL BASED ON NONLINEARITY COMPENSATION AND THE IMPROVED SMO STRATEGY

1) GIVEN SPEED IS 10RPM

Without the nonlinearity compensation, the waveforms of the speed, estimated back EMF/H, three-phase currents and the FFT analysis are shown in Figure 18 while the corresponding waveforms with nonlinearity compensation are given in Figure 19.

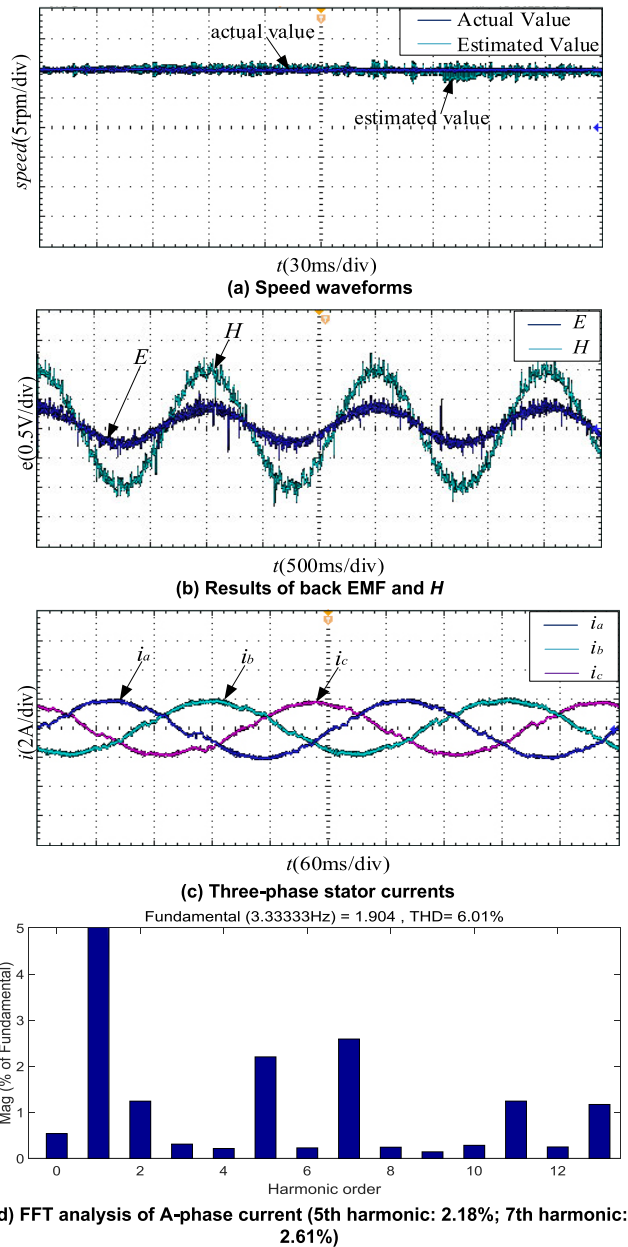


FIGURE 19. Results with nonlinearity compensation.

2) GIVEN SPEED IS 50RPM

Similarly, without the nonlinearity compensation, the waveforms of the speed, three-phase currents and the FFT analysis are shown in Figure 20 while the corresponding waveforms with nonlinearity compensation are given in Figure 21.

With the nonlinearity compensation being added to the improved SMO, the harmonic components in the stator currents significantly decrease from approximately 8.06% to 6.01% (5th harmonic: 4.08% to 2.18%; 7th harmonic: 4.11% to 2.61%) when the given speed is 10 rpm and from 7.03% to 3.87% (5th harmonic: 4.62% to 1.71%; 7th harmonic: 4.36% to 1.77%) when the given speed is 50 rpm. The estimation performances of the back EMF and the rotor

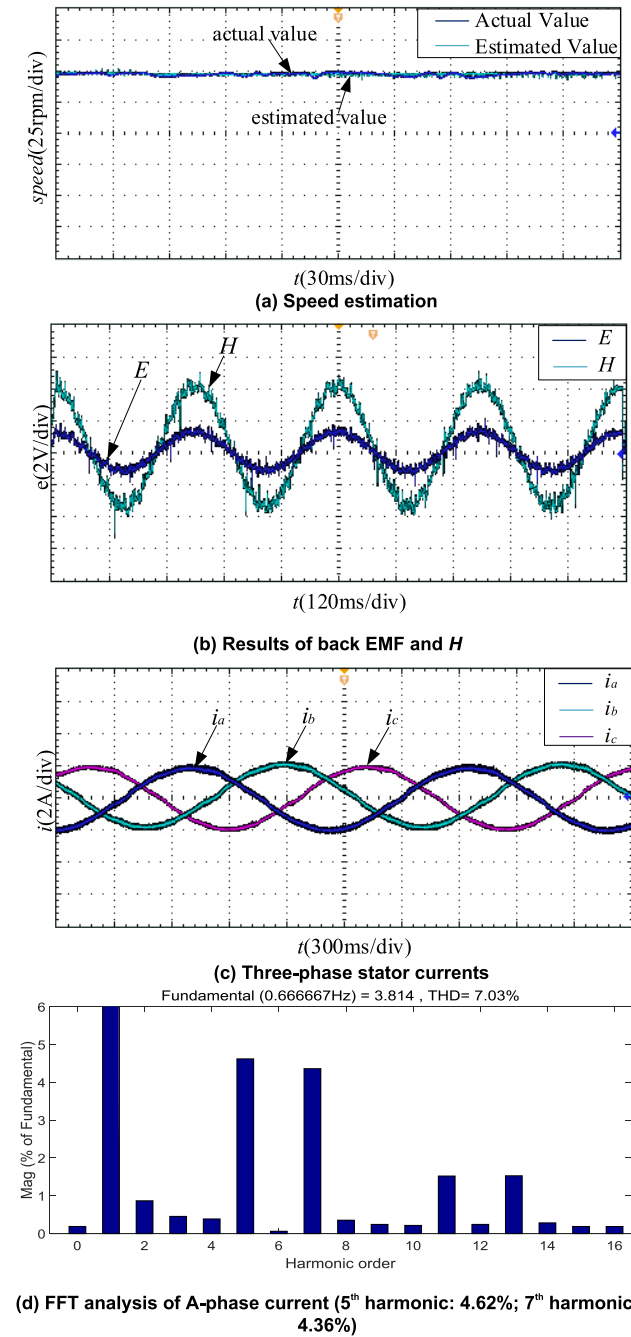


FIGURE 20. Results without nonlinearity compensation.

position are also improved because of the better stator current performance.

To further test the applicability of this proposed method, different low-speed conditions (from 5 rpm to 50 rpm) are also been tested, and the corresponding results are summarized in TABLE 4.

It is obvious that lower speed means a lower back EMF value and the estimation accuracy is apparently reduced, e.g., when the speed is 5 rpm, this proposed method still works; however, the estimation accuracy reduces to 40%, while the estimation accuracy is 6% at 50 rpm.

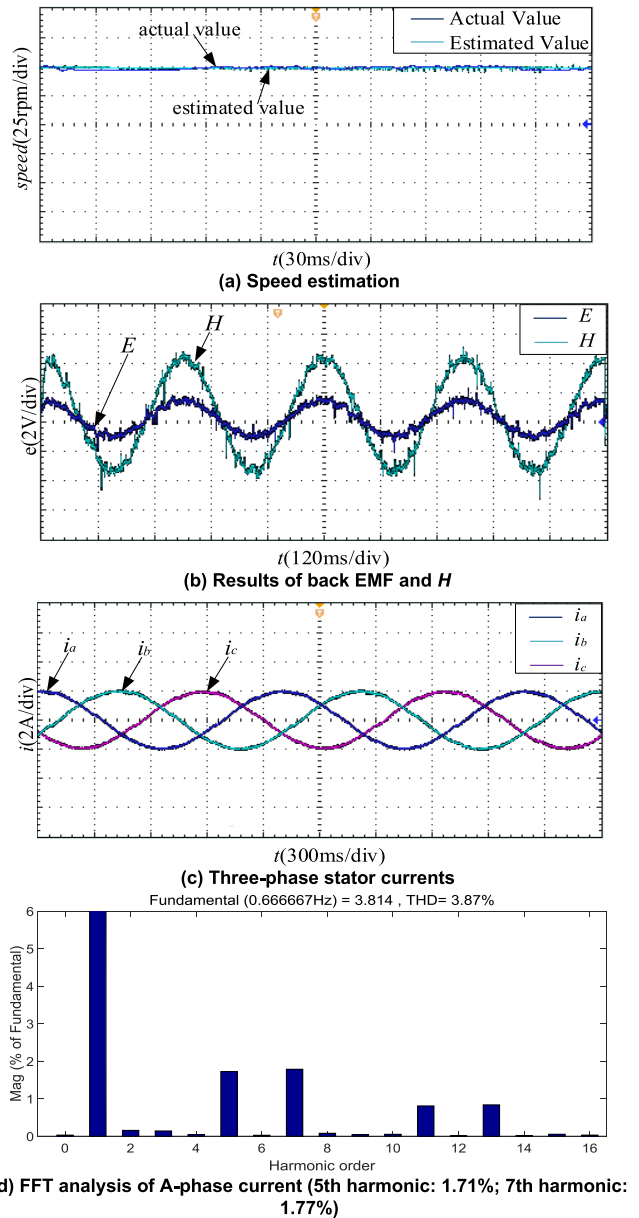


FIGURE 21. Results with nonlinearity compensation.

TABLE 4. Estimated results for different speeds.

Speed(rpm)	Back EMF(V)	Δn (rpm)	Error rate(%)
50	1.6	3	6
10	0.32	1.5	15
9	0.288	2	22.22
8	0.256	2	25
5	0.16	2	40

V. CONCLUSION

In this paper, a novel sensorless control strategy was studied for the SPMSM with low-speed conditions. Through the introduction of an intermediate variable H , the estimation

accuracy of the rotor position was improved at low speed as the back EMF value was extended, and the inherent chattering was also reduced through the redesign of the sliding switching function. In addition, with the newly designed harmonic extraction method named GSDFT, a voltage compensation link was added to compensate for the harmonic components in the three-phase stator currents because of inverter nonlinearity. This nonlinearity compensation could not only reduce the stator harmonic distortion but also improve the estimation accuracy of the rotor position.

With this novel control strategy, the rotor estimation accuracy could be restricted within ± 3 rpm and ± 1.5 rpm, and the THD of the stator current reduced from 7.03% to 3.87% and 8.06% to 6.01% when the rotor speeds were 50 rpm and 10 rpm, respectively, and even when the rotor speed was as low as 5 rpm, this novel method could also work, but the accuracy reduced 40%. The execution time of this method was much shorter than the SDFT compensation method. In the future, research work on rotor position estimation at zero speed/large torque or a very low speed should be carried out in depth.

REFERENCES

- [1] H. Li, D. Ke, R. Zu, P. Tao, and F. Wang, "Sensorless control of permanent magnet synchronous motor based on an improved sliding mode observer," in *Proc. IEEE Student Conf. Electr. Mach. Syst.*, HuZhou, China, Dec. 2018, pp. 1–6.
- [2] Q. Yuan, H. Wu, J. Qian, and B. Zhang, "Research on sensorless control of permanent magnet synchronous motor based on novel sliding mode observer," in *Proc. Asia-Pacific Magn. Recording Conf. (APMRC)*, Shanghai, China, Nov. 2018, pp. 1–2.
- [3] D. Guan, M. X. Bui, D. Xiao, and M. F. Rahman, "Sensorless control interior permanent-magnet synchronous motor drive over wide speed range operation based on the current derivative method," in *Proc. 20th Int. Conf. Electr. Mach. Syst. (ICEMS)*, Sydney, NSW, Australia, Aug. 2017, pp. 1–6.
- [4] X. Tongxing, W. Xiaolin, L. Yuting, and Z. Hang, "Position estimation method based on frequency self-optimization high-frequency signal injection," in *Proc. 22nd Int. Conf. Electr. Mach. Syst. (ICEMS)*, Harbin, China, Aug. 2019, pp. 1–4.
- [5] S. C. Xing and W. Chen, "Sensorless control of three-phase permanent magnet synchronous motor based on fundamental wave mathematical model," in *Proc. 2nd Int. Conf. Cybern., Robot. Control (CRC)*, Chengdu, China, Jul. 2017, pp. 89–93.
- [6] X. Sun, J. Cao, G. Lei, Y. Guo, and J. Zhu, "Speed sensorless control for permanent magnet synchronous motors based on finite position set," *IEEE Trans. Ind. Electron.*, vol. 67, no. 7, pp. 6089–6100, Jul. 2020.
- [7] X. Sun, L. Chen, Z. Yang, and H. Zhu, "Speed-sensorless vector control of a bearingless induction motor with artificial neural network inverse speed observer," *IEEE/ASME Trans. Mechatronics*, vol. 18, no. 4, pp. 1357–1366, Aug. 2013.
- [8] G. Tian, X. Feng, Y. Yan, Z. Y. Ru, and Z. X. Peng, "Research on rotor position estimation method of sensorless permanent magnet synchronous motor," in *Proc. 2nd IEEE Adv. Inf. Manage., Communicates, Electron. Automat. Control Conf. (IMCEC)*, Xi'an, China, May 2018, pp. 714–717.
- [9] L. Yan, Y. Liao, H. Lin, and J. Sun, "Torque ripple suppression of permanent magnet synchronous machines by minimal harmonic current injection," *IET Power Electron.*, vol. 12, no. 6, pp. 1368–1375, May 2019.
- [10] Q. Zhang, J. Zhang, and Y. Wang, "Sliding-mode control for singular Markovian jump systems with Brownian motion based on stochastic sliding mode surface," *IEEE Trans. Syst., Man, Cybern., Syst.*, vol. 49, no. 3, pp. 494–505, Mar. 2019.
- [11] D. Liang, J. Li, and R. Qu, "Sensorless control of permanent magnet synchronous machine based on second-order sliding-mode observer with online resistance estimation," *IEEE Trans. Ind. Appl.*, vol. 53, no. 4, pp. 3672–3682, Jul./Aug. 2017.
- [12] A. Cichowski and J. Nieznanski, "Self-tuning dead-time compensation method for voltage-source inverters," *IEEE Power Electron Lett.*, vol. 3, no. 2, pp. 72–75, Jun. 2005.
- [13] S.-Y. Kim and S.-Y. Park, "Compensation of dead-time effects based on adaptive harmonic filtering in the vector-controlled AC motor drives," *IEEE Trans. Ind. Electron.*, vol. 54, no. 3, pp. 1768–1777, Jun. 2007.
- [14] J. Xinhai, L. Baisong, and X. Dianguo, "A current harmonics suppression method for permanent magnet synchronous motor drives," in *Proc. IEEE Transp. Electrific. Conf. Expo. Asia-Pacific (ITEC Asia-Pacific)*, Harbin, China, Aug. 2017, pp. 1–6.
- [15] G. Liu, B. Chen, K. Wang, and X. Song, "Selective current harmonic suppression for high-speed PMSM based on high-precision harmonic detection method," *IEEE Trans. Ind. Informat.*, vol. 15, no. 6, pp. 3457–3468, Jun. 2019.
- [16] K. Yamanaka, T. Ohnishi, and M. Hojo, "A novel position sensorless vector control of permanent-magnet synchronous motors," in *Proc. Power Convers. Conf. Nagoya*, Nagoya, Japan, Apr. 2007, pp. 290–295.
- [17] X. Li, Z. Xie, and J. Luo, "Iterative windowed interpolation FFT harmonic analysis method," *J. Power Syst. Automat.*, vol. 31, no. 2, pp. 32–37, 2019.
- [18] E. Jacobsen and R. Lyons, "The sliding DFT," *IEEE Signal Process. Mag.*, vol. 20, no. 2, pp. 74–80, Mar. 2003.
- [19] Q.-Q. Yuan, X.-J. Wu, and P. Dai, "Rotor initial position estimation based on sDFT for electrically excited synchronous motors," *J. Power Electron.*, vol. 14, no. 3, pp. 564–571, May 2014.
- [20] H. Liu, H. Hu, H. Chen, L. Zhang, and Y. Xing, "Fast and flexible selective harmonic extraction methods based on the generalized discrete Fourier transform," *IEEE Trans. Power Electron.*, vol. 33, no. 4, pp. 3484–3496, Apr. 2018.
- [21] L. Yuan, *Modern Permanent Magnet Synchronous Motor Control Principle and MATLAB Simulation*. Beijing, China: Beijing Aerospace Univ. Press, 2016.
- [22] S. Chi and L. Xu, "Position sensorless control of PMSM based on a novel sliding mode observer over wide speed range," in *Proc. 5th Int. Power Electron. Motion Control Conf.*, Shanghai, China, Aug. 2006, pp. 1–7.
- [23] J. Lee, S. Lim, I. Kim, W. Jeong, S. Park, and H. Yang, "An adaptive disturbance rejection method with stability enhancement using adjustable dead zone for hard disk drives," *IEEE Trans. Magn.*, vol. 53, no. 3, Mar. 2017, Art. no. 8000409.
- [24] N. Urasaki, T. Senjyu, K. Uezato, and T. Funabashi, "An adaptive dead-time compensation strategy for voltage source inverter fed motor drives," *IEEE Trans. Power Electron.*, vol. 20, no. 5, pp. 1150–1160, Sep. 2005.
- [25] S.-Y. Kim, W. Lee, M.-S. Rho, and S.-Y. Park, "Effective dead-time compensation using a simple vectorial disturbance estimator in PMSM drives," *IEEE Trans. Ind. Electron.*, vol. 57, no. 5, pp. 1609–1614, May 2010.



QINGQING YUAN was born in 1987. She received the B.S., M.S., and Ph.D. degrees from the China University of Mining and Technology, China, in 2009, 2011, and 2014, respectively. Since 2014, she has been with the Department of Electrical Engineering, University of Shanghai for Science and Technology, China, where she is currently a Teacher. Her current research interests include motor control and new energy technology applications.



YUMEI YANG was born in China, in 1995. She received the B.Eng. degree from the Department of Electrical Engineering, Qingdao University (QDU), Qingdao, China, in 2018. She is currently pursuing the M.Eng. degree with the Electrical Engineering Department, University of Shanghai for Science and Technology (USST). Her current research interests include motor control and deep learning.



HAODONG WU was born in China, in 1995. He received the B.Eng. degree from the Department of Electrical Engineering, University of Shanghai for Science and Technology (USST), Shanghai, China, in 2017. He is currently pursuing the M.Eng. degree with the Electrical Engineering Department, USST. His current research interests include motor control and deep learning.



HUI WU was born in 1984. He received the B.S. degree from the China University of Mining and Technology, in 2006, and the B.S. and M.S. degrees from the University of Duisburg-Essen, Germany, in 2007 and 2010, respectively. In 2010, he started working with the China Coal Technology and Engineering Group. He is currently an Associate Scientist and engaged in research in control theory and control engineering.

...